



Full Length Article

## Characterization of CLLBC scintillation detector response to $\gamma$ -rays and neutrons

Elias Arnqvist <sup>a</sup>,\* Stephan Oberstedt <sup>b</sup>, Ali Al-Adili <sup>a</sup>, Cristiano Lino Fontana <sup>b</sup>,  
Alessandro Borella <sup>c</sup>, Riccardo Rossa <sup>c</sup>, Wouter Geerts <sup>b</sup>, Miguel Macías <sup>b</sup>, Marzio Vidali <sup>b</sup>,  
Andreas Oberstedt <sup>d</sup>, Mattias Lantz <sup>a</sup>

<sup>a</sup> Department of Physics and Astronomy, Uppsala University, Box 516, Uppsala, 75120, Sweden

<sup>b</sup> European Commission, Joint Research Centre (JRC), Retieseweg 111, Geel, 2440, Belgium

<sup>c</sup> SCK CEN, Belgian Nuclear Research Center, Boeretang 200, Mol, 2400, Belgium

<sup>d</sup> Extreme Light Infrastructure - Nuclear Physics (ELI-NP), Horia Hulubei National Institute for R&D in Physics and Nuclear Engineering (IFIN-HH), Strada Reactorului 30, Bucharest-Magurele, 077125, Romania

### ARTICLE INFO

#### Keywords:

CLLBC  
Elpasolite  
AmBe  
Neutron tagging  
Time-of-flight

### ABSTRACT

The dual-mode elpasolite scintillation material CLLBC ( $\text{Cs}_2\text{LiLaBr}_{4.8}\text{Cl}_{1.2}:\text{Ce}$ ) is capable of measuring both  $\gamma$ -rays and neutrons. The neutron detection capability spans from thermal energies up to about 10 MeV, making these detectors attractive options for studying prompt fission neutron spectra (PFNS). In this work, a comprehensive characterization of CLLBC detectors is performed. Three CLLBC detectors were characterized, in addition to three  $\text{LaBr}_3:\text{Ce}$  and two  $\text{LaBr}_3:\text{Ce},\text{Sr}$  for comparison. For the best-performing CLLBC detector, the results indicate an energy resolution of 3.7% at  $E_\gamma = 662$  keV and an intrinsic timing resolution of 1.2 ns (FWHM) above  $E_\gamma = 1$  MeV using  $^{60}\text{Co}$ . A  $\gamma$ -neutron separation figure-of-merit of 2.7 is obtained by means of pulse-shape discrimination. Tagged neutron time-of-flight measurements were conducted using a  $^{241}\text{Am}^9\text{Be}$  neutron source, by coincident detection of the 4.44 MeV  $\gamma$ -ray and the neutron, to determine the intrinsic neutron detection efficiency between 2–6 MeV. Neutron detection efficiencies of about 0.2% for the  $^6\text{Li}(n,t)^4\text{He}$  reaction and 1% for three types of  $(n,n')$  reactions were obtained. Two of three investigated CLLBC detectors exhibit an energy peak asymmetry, resulting in worse performance, indicating scintillator quality issues and motivating further investigation. Future studies are anticipated using the  $^{252}\text{Cf}(\text{sf})$  prompt fission neutron spectrum to determine neutron efficiencies for a wider range of neutron energies. Although observed in a previous study, neutron detection via  $^{35}\text{Cl}(n,p)^{35}\text{S}$  was not identified in this work but is planned to be determined using quasi-monoenergetic neutrons generated at the JRC MONNET facility.

### 1. Introduction

Scintillation materials from the elpasolite crystal family were recently developed and brought to market. One such scintillator is CLLBC ( $\text{Cs}_2\text{LiLaBr}_{4.8}\text{Cl}_{1.2}:\text{Ce}$ ) [1] which is sensitive to  $\gamma$ -rays and neutrons from thermal energies up to about 10 MeV. Like for some other elpasolites [2–4], neutrons are mainly detected through reactions on  $^6\text{Li}$  and  $^{35}\text{Cl}$ , which can be combined with pulse-shape discrimination (PSD) to separate the detection of neutrons from  $\gamma$ -rays.

Another detection mechanism is through  $\gamma$ -rays produced in the detector following  $(n,n')$  reactions induced by neutrons, an idea suggested by Oberstedt et al. [5] and developed further by Ebran et al. [6]. With  $\text{LaBr}_3:\text{Ce}$  detectors, the detection of neutrons down to about 170 keV is possible with this method [5,6], an energy inaccessible with standard

liquid scintillation detectors [7]. CLLBC contains the elements present in  $\text{LaBr}_3:\text{Ce}$ , thus allowing for this detection mechanism.

At the European Commission's Joint Research Centre in Geel, Belgium (JRC-Geel), a variety of scintillation detectors have been used for nuclear fission research for more than a decade. In particular, as requested by the Nuclear Energy Agency [8], these detectors have been used in the assessment of prompt fission  $\gamma$ -ray energy spectra (PFGS) and average multiplicities from a variety of fission reactions [9–19].

Thanks to a wide energy range of neutron detection, PSD capabilities, and a good energy resolution, the possibility of utilizing CLLBC detectors for simultaneous  $\gamma$ -ray and neutron measurements is attractive for fission research at JRC-Geel. Importantly, CLLBC appears suitable

\* Corresponding author.

E-mail address: [elias.arnqvist@physics.uu.se](mailto:elias.arnqvist@physics.uu.se) (E. Arnqvist).

<https://doi.org/10.1016/j.nima.2025.170470>

Received 3 February 2025; Received in revised form 17 March 2025; Accepted 24 March 2025

Available online 18 April 2025

0168-9002/© 2025 The Authors. Published by Elsevier B.V. This is an open access article under the CC BY license (<http://creativecommons.org/licenses/by/4.0/>).

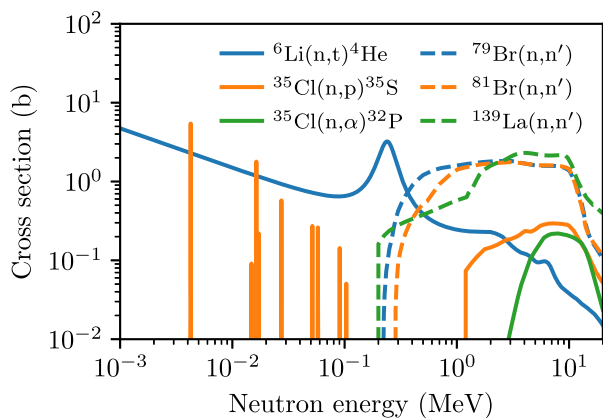


Fig. 1. Cross sections of selected neutron detection reactions in CLLBC. Data is from ENDF/B-VIII.0 [20].

for determining prompt fission neutron spectra (PFNS) and how neutrons correlate with fission-fragment characteristics. The broad energy range for neutron sensitivity of CLLBC is crucial to capture the entire PFNS. Cross sections for reactions responsible for neutron detection in CLLBC are shown in Fig. 1.

However, only a few limited characterizations of CLLBC detectors can be found in literature [1,21–27] that do not measure neutron detection efficiencies and intrinsic timing resolutions, properties crucial for neutron time-of-flight (ToF) applications. In the following, a comprehensive CLLBC characterization is reported, including pulse-height calibration, energy resolution, intrinsic timing resolution, and the intrinsic detection efficiency for  $\gamma$ -rays and neutrons. An  $^{241}\text{Am}^9\text{Be}$  neutron source was employed for tagged neutron ToF measurements to determine the neutron efficiency between 2–6 MeV. Obtained characteristics are compared to those of  $\text{LaBr}_3:\text{Ce}$  detectors, which also were investigated here and in a previous study [28].

## 2. Experiment details

The detector characterization was performed using the VESPA (Versatile Spectrometry Array) setup at JRC-Geel [19]. Three CLLBC detectors of two sizes manufactured by SCIONIX [29] were characterized. Additionally, three  $\text{LaBr}_3:\text{Ce}$  and two  $\text{LaBr}_3:\text{Ce},\text{Sr}$  detectors were included for comparison and for tagging neutrons. The geometric details of the setup are shown to scale in Fig. 2 and presented in Table 1.

For  $\gamma$ -ray response characterization, standard sources between 80 keV and 6.13 MeV were used, covering the dynamical range typical for PFGS. For high-energy  $\gamma$ -rays, escape peaks could also be utilized for some measurements. In some cases X-rays were used, extending

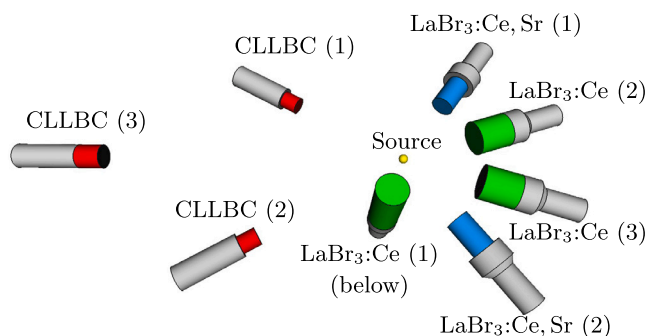


Fig. 2. Detector setup used in this work, shown to scale.

Table 1

Properties of detectors used in this work, including detector type, detector number # (when more than one of a type), sizes of detector crystals (diameter  $\times$  length), identifiers (serial No.), distances to the  $\gamma$ -ray or neutron source, and the bias voltages applied to the photomultipliers.

Detector type	#	$\phi \times \text{length}$ (mm $\times$ mm)	serial No.	dist. (mm)	bias (V)
CLLBC	1	38.1 $\times$ 38.1	S1AA7702	270	-810
CLLBC	2	38.1 $\times$ 38.1	S1AA7703	349	-760
CLLBC	3	50.8 $\times$ 50.8	S2AC1151 <sup>a</sup>	650	790
$\text{LaBr}_3:\text{Ce}$	1	76.2 $\times$ 76.2	A14400	170	539
$\text{LaBr}_3:\text{Ce}$	2	76.2 $\times$ 76.2	A14401	170	539
$\text{LaBr}_3:\text{Ce}$	3	88.9 $\times$ 203.2	A11218	246	700
$\text{LaBr}_3:\text{Ce},\text{Sr}$	1	50.8 $\times$ 76.2	A20321	170	626
$\text{LaBr}_3:\text{Ce},\text{Sr}$	2	50.8 $\times$ 76.2	A20322	170	620

<sup>a</sup> Owner: SCK CEN, Belgian Nuclear Research Center.

Table 2

Calibration sources used, their activity or neutron strength at the time of measurement, and energies of strong  $\gamma$ - or X-ray emissions.

Isotope	Activity/ strength	$E_\gamma$ or $E_{\text{X-ray}}$ (keV)
$^{60}\text{Co}$	18.7 kBq	1173, 1332
$^{133}\text{Ba}$	21.3 kBq	81, 276, 303, 356, 384
$^{137}\text{Cs}$	29.6 kBq	32, 662
$^{152}\text{Eu}$	22.5 kBq	122, 245, 344, 411, 444, 779 964, 1112
$^{207}\text{Bi}$	34.4 kBq	73, 570, 1064, 1770
$^{232}\text{Th}$	Unknown	238, 463, 511, 583, 727, 911 968, 2615
$^{238}\text{Pu}^{13}\text{C}$	$6.5 \cdot 10^4$ n/s	6130
$^{241}\text{Am}^9\text{Be}$	$3.0 \cdot 10^3$ n/s	60, 4439
$^{241}\text{Am}^9\text{Be}$	$7.6 \cdot 10^4$ n/s	60, 4439

the range down to 32 keV. For the neutron response characterization,  $^{238}\text{Pu}^{13}\text{C}$  and  $^{241}\text{Am}^9\text{Be}$  radionuclide ( $\alpha,n$ ) sources were used. All sources are listed in Table 2.

The data acquisition system (DAQ) was based on a CAEN DT5730SB [30] digitizer with eight input channels, a 500 MS/s sampling rate, and a 14-bit precision. A personal computer was connected to the digitizer via an optical link and CAEN A4818 USB 3.0 adapter. The data acquisition framework ABCD [31] was utilized to handle waveform analysis. Each waveform was digitized and the following was recorded: input channel, full pulse integral by integrating the pulse, timestamp by using constant-fraction timing (CFD), and PSD parameter by taking the fraction of partial integrals. To calculate the PSD parameter, the integral of the first part of the pulse,  $Q_1$ , was compared to the integral of the last part of the pulse,  $Q_2$ , using the parameter  $\text{PSD} = Q_1/Q_2$ . This resulted in an ability to discriminate between the pulse shapes caused by different detection reactions. User-specified parameters used in the full pulse integral, CFD, and PSD algorithms were optimized to achieve the best energy resolution, time resolution, and PSD FoM (figure-of-merit). An in-depth description of waveform analysis algorithms used in ABCD is discussed by Fontana et al. [32].

Waveform analysis was performed with ABCD for the majority of this detector characterization. However, to accommodate a higher count rate while avoiding any potential dead time losses when performing tagged-neutron ToF, the digitizer onboard FPGA (Field-Programmable Gate Array) was used. Although the FPGA is less flexible in the specific analysis algorithms, it offers benefits in situations where the speed of the digitizer-PC connection is limiting. However, the FPGA used the formula  $\text{PSD} = Q_2/(Q_1 + Q_2)$  and a different CFD algorithm.

## 3. Results and discussion

In this section, the results of the CLLBC detector characterization are presented and discussed.

### 3.1. Energy calibration and resolution

Using the sources listed in Table 2, the full pulse integral was measured as a function of  $\gamma$ -ray (or X-ray) energy  $E_\gamma$  from 32 keV to 6.1 MeV. This data is presented in Fig. 3 for the three CLLBC detectors. Least-square fitting was performed on the data with different calibration functions. A cubic function proved to fit sufficiently well and was selected for use. The residual of the cubic fit ( $E_\gamma - E_{\gamma,fit}$ ) was divided by  $E_\gamma$ , allowing for direct comparison with the energy resolution. These residuals are shown in Fig. 3. Also shown is a function on the form  $a/\sqrt{E_\gamma}$  corresponding to the statistical contribution of an energy resolution of  $R_{FWHM} = 3\%$  at  $E_\gamma = 662$  keV, for comparison. This resolution is, with some margin, representative of CLLBC detectors. Since the residuals all lie within the  $R_{FWHM} = 3\%$  region, the calibration is deemed appropriate.

The energy resolutions  $R_{FWHM}$  of the CLLBC detectors were also investigated using the  $\gamma$ -ray sources, except for the 4.44 MeV AmBe  $\gamma$ -ray as it is affected by Doppler broadening [33]. Acquired spectra were analyzed with InterSpec [34], where each peak was fit with a Gaussian on a linear background. The resulting FWHM (full-width-at-half-maximum) was divided by  $E_\gamma$ , to obtain  $R_{FWHM}$  for each peak. The results are shown in Fig. 4 for all CLLBC detectors and one LaBr<sub>3</sub>:Ce for comparison. Error bars were obtained from the Gaussian fitting of the peak. Also shown are fits on the form  $\sqrt{a^2 + b^2 E_\gamma/E_\gamma}$ , as suggested by literature [35].

Values of  $R_{FWHM}$  at  $E_\gamma = 662$  keV are about 5.7%, 3.7%, and 4.8% for CLLBC detectors 1–3. Out of the investigated CLLBC detectors, CLLBC 2 thus has a better resolution than 1 and 3. This difference is primarily explained by an energy peak asymmetry observed for detectors 1 and 3. The asymmetry is illustrated by Fig. 5 and is probably a result of inhomogeneities in the crystal, such as in doping concentration or manufacturing defects. Nevertheless, the performance of the best-performing CLLBC is similar to those previously measured by others

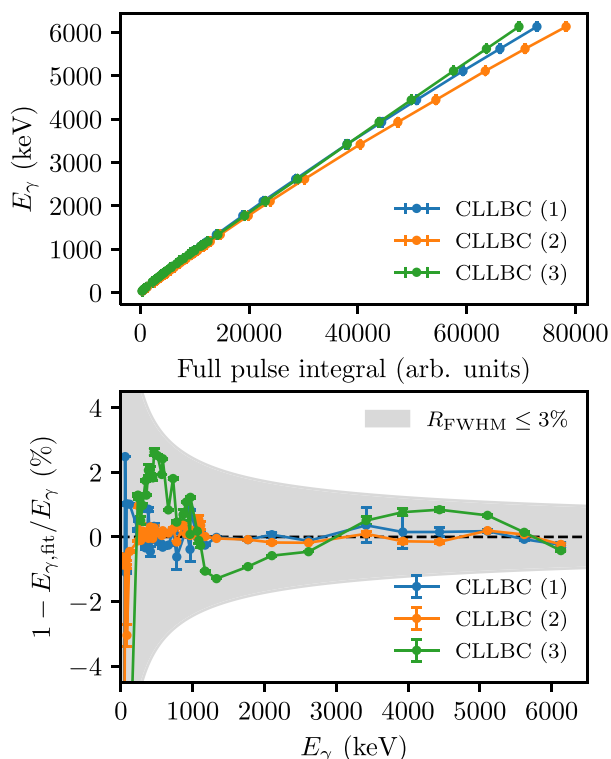


Fig. 3. Top: calibration curve of the  $\gamma$ -ray response of the CLLBC detectors. Bottom: residuals using a cubic calibration function compared to  $R_{FWHM} \leq 3\%$ .

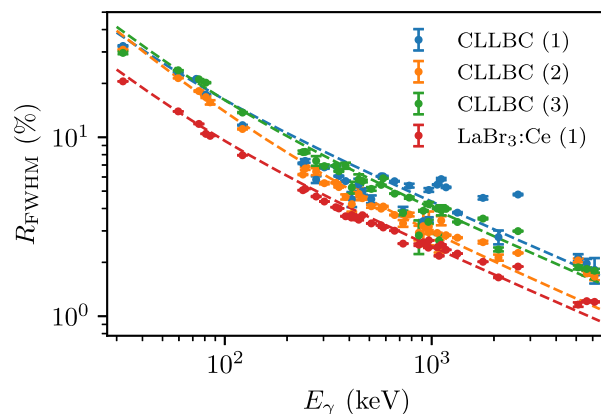


Fig. 4. Energy resolution as a function of  $\gamma$ -ray energy for the CLLBC detectors and one LaBr<sub>3</sub>:Ce detector. Dashed lines are fit based on expected behavior.

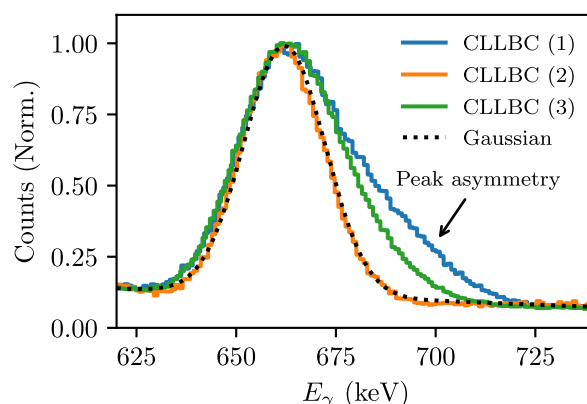


Fig. 5. Peak at  $E_\gamma = 662$  keV measured with CLLBC detectors, illustrating the asymmetry exhibited by two detectors. A Gaussian peak on a linear background is shown for comparison.

(3.0% [1], 4.1% [21], and 2.9% [22]). As measurements of PFGS and PFNS are the planned use case of these detectors, a large dynamic range of  $E_\gamma$  was prioritized over the best  $R_{FWHM}$ . Compared to CLLBC, the LaBr<sub>3</sub>:Ce detector featured a better  $R_{FWHM}$  of 2.9% at 662 keV.

### 3.2. Detection efficiency for $\gamma$ rays

Both absolute and intrinsic peak efficiencies were determined for the CLLBC detectors using selected intense  $\gamma$ -ray peaks. Simulations were performed in Geant4 [36–38] for comparison and scaled with a constant to the measured data using least-squares fitting. Scaling was done to account for losses that had not been modeled. Dead time corrections were applied by fitting time interval distributions [39] and were found to be  $<5\%$ . For some  $\gamma$ -ray peaks, a background subtraction was performed. For the AmBe source, only the neutron emission rate was known. A  $\gamma/n$  ratio of  $0.6 \pm 0.1$  was assumed, based on previous investigations [40]. The activity of the Th source was unknown, but to get data at  $E_\gamma = 2.6$  MeV ( $^{208}\text{Tl}$ , a daughter of  $^{232}\text{Th}$ ), an interpolation of the efficiency at  $E_\gamma = 583$  keV ( $^{208}\text{Tl}$ ) was first performed using data at  $E_\gamma = 570$  keV ( $^{207}\text{Bi}$ ) and  $E_\gamma = 662$  keV ( $^{137}\text{Cs}$ ). By multiplying the interpolated efficiency by the fraction of peak counts at 2.6 MeV to 583 keV and the fraction of  $^{208}\text{Tl}$   $\gamma$ -ray intensity at 583 keV to 2.6 MeV, an estimate for the efficiency at 2.6 MeV was obtained. In all cases, uncertainties were propagated accordingly. Intrinsic peak efficiencies are shown in Fig. 6.

The intrinsic peak efficiency of the detectors is highest around  $E_\gamma = 100$  keV. Below this absorption in the detector enclosure becomes significant, and above this interactions through photoelectric absorption

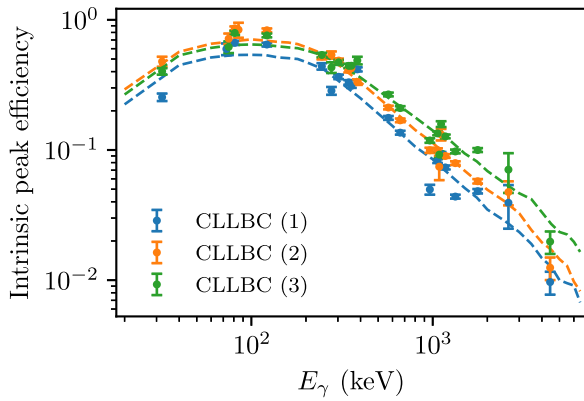


Fig. 6. Intrinsic peak efficiencies as a function of  $\gamma$ -ray energy of the CLLBC detectors. Dashed lines are from Geant4 simulations.

become less likely. Measured data agree well with Geant4 simulations over the whole  $E_\gamma$  range. Some difference is seen between the CLLBC detectors, even those of the same size. Interestingly, the detectors that exhibit asymmetry have lower efficiencies, which could either be caused directly by the same issue as the asymmetry or indirectly by the area calculations of asymmetric peaks. CLLBC 3 is 1/3 larger than 1 and 2, which is reflected in higher efficiencies at high  $E_\gamma$ .

### 3.3. Timing resolution

To determine intrinsic timing resolutions of the detectors, coincidence measurements of a  $^{60}\text{Co}$  source were performed. Through coincident detection of the nearly simultaneously ( $<1$  ps) emitted 1173 keV and 1332 keV  $\gamma$ -rays in two detectors, the combined timing resolution was obtained for the detector pair (A and B) as the FWHM of the time difference distribution,  $\sigma_{\text{AB}}$ . This is related to the intrinsic timing resolutions of the detectors A and B as  $\sigma_{\text{AB}}^2 = \sigma_{\text{A}}^2 + \sigma_{\text{B}}^2$  [28]. For each combination of detectors (8 detectors, 28 unique pairs), pairwise timing resolutions were determined, and an overdetermined system of linear equations was formed. Uncertainty-weighted least squares fitting was then performed to obtain intrinsic timing resolutions for all of the detectors.

Traditionally, an assumption of two detectors having the same intrinsic timing resolution has to be made to solve the system of equations and obtain intrinsic timing resolutions [28]. However, the method employed here has benefits in situations where the assumption of identical detectors cannot be made and may be useful for future applications.

An energy cut was imposed to remove detection events below a threshold  $E_{\gamma,\text{cut}}$ . The main purpose of this was to remove contributions from Compton scattering between detectors, which worsens the timing resolution. The intrinsic timing resolutions of the CLLBC detectors are

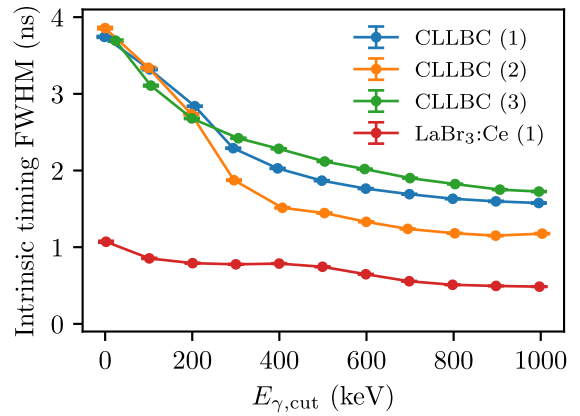


Fig. 7. Intrinsic FWHM timing resolutions as a function of lower  $\gamma$ -ray energy cut for the CLLBC detectors, when measuring  $^{60}\text{Co}$ . Corresponding results for a  $\text{LaBr}_3:\text{Ce}$  detector are shown for comparison.

presented in Fig. 7 as a function of  $E_{\gamma,\text{cut}}$ . Results for a  $\text{LaBr}_3:\text{Ce}$  detector is shown for comparison.

Results show that the intrinsic timing resolution improves with higher  $E_{\gamma,\text{cut}}$ , as Compton scattered gammas are excluded and there is an approximate dependence of  $\text{FWHM} \propto 1/\sqrt{E_{\gamma,\text{cut}}}$  [28]. For  $^{60}\text{Co}$ , the values obtained at  $E_{\gamma,\text{cut}} = 1$  MeV are thus seen as the most accurate. The timing resolutions of the CLLBC detectors are at best about 1.2 ns, but the two detectors exhibiting peak asymmetry perform slightly worse, at around 1.6–1.7 ns. This timing resolution is good, but the  $\text{LaBr}_3:\text{Ce}$  detector performs better at less than 500 ps. Especially at low  $E_{\gamma,\text{cut}}$ , the better  $\text{LaBr}_3:\text{Ce}$  performance is clear compared to CLLBC. A summary of all  $\gamma$ -ray detection characteristics is shown in Table 3.

### 3.4. Response to neutrons

The response of the CLLBC detectors to neutrons is presented and discussed in this section.

#### 3.4.1. Thermal-neutron detection via the $^6\text{Li}(n,t)$ reaction

The thermal-neutron cross section of  $^6\text{Li}(n,t)$  is very large, making this a suitable detection channel for low-energy neutrons. To study the PSD capabilities of CLLBC for the separation of  $\gamma$ -rays and neutrons through the  $^6\text{Li}(n,t)$  reaction, a  $^{238}\text{Pu}^{13}\text{C}$  neutron source was measured. The PuC source was not moderated but a significant low-energy neutron flux was still emitted and further thermalized from neutron scattering in the environment. To determine the  $\gamma$ -neutron peak separation, a FoM was used, which was defined as

$$\text{FoM}_{\gamma n} = \frac{|X_\gamma - X_n|}{\text{FWHM}_\gamma + \text{FWHM}_n}, \quad (1)$$

Table 3

Summary of  $\gamma$ -ray characteristics of CLLBC and  $\text{LaBr}_3$  detectors, including energy resolutions  $R_{\text{FWHM}}$ , intrinsic FWHM timing resolutions  $\Delta t$  for  $^{60}\text{Co}$ , and absolute peak detection efficiencies at  $E_\gamma = 4.4$  MeV.

Detector type	#	serial No.	$R_{\text{FWHM}}$ at $E_\gamma = 662$ keV (%):			$\Delta t$ at $E_{\gamma,\text{cut}} = 1$ MeV (ps):		$\epsilon_{\gamma,\text{abs}} \times 10^3$ at $E_\gamma = 4.4$ MeV
			Measured	Specified	From [28]	Measured	From [28]	
CLLBC	1	S1AA7702	$5.68 \pm 0.02$	3.4	–	$1576 \pm 8$	–	$0.013 \pm 0.005$
CLLBC	2	S1AA7703	$3.68 \pm 0.02$	3.2	–	$1177 \pm 8$	–	$0.009 \pm 0.003$
CLLBC	3	S2AC1151	$4.84 \pm 0.01$	3.3	–	$1726 \pm 7$	–	$0.042 \pm 0.015$
$\text{LaBr}_3:\text{Ce}$	1	A14400	$2.92 \pm 0.01$	3.0	3.0	$485 \pm 4$	$562 \pm 8$	$0.96 \pm 0.33$
$\text{LaBr}_3:\text{Ce}$	2	A14401	$3.01 \pm 0.01$	2.7	3.0	$487 \pm 4$	$562 \pm 8$	$0.92 \pm 0.32$
$\text{LaBr}_3:\text{Ce}$	3	A11218	$3.34 \pm 0.01$	2.7	3.5	$865 \pm 3$	$823 \pm 10$	$1.33 \pm 0.46$
$\text{LaBr}_3:\text{Ce,Sr}$	1	A20321	$2.32 \pm 0.01$	2.10	–	$478 \pm 4$	–	$0.30 \pm 0.10$
$\text{LaBr}_3:\text{Ce,Sr}$	2	A20322	$2.37 \pm 0.01$	2.15	–	$458 \pm 4$	–	$0.31 \pm 0.11$

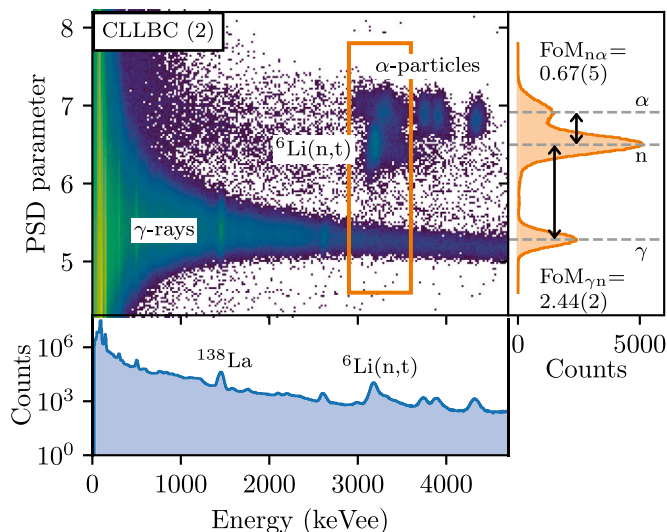


**Fig. 8.** PSD parameter vs. energy histogram from a measurement of a PuC source with CLLBC detector 2. Note that the energy is  $\gamma$ -equivalent and in units of keVee (electron equivalent). Projections of the data are shown on both the energy and PSD axis. The FoM for  $\gamma$ -neutron and neutron- $\alpha$  separation are shown, for neutron detection through the  ${}^6\text{Li}(n,t)$  reaction. Waveform analysis was performed with ABCD.

where  $X$  denotes the peak positions and FWHM refers to the widths at peak positions. The PSD parameter FoM for  $\gamma$ -neutron and neutron- $\alpha$  separation was investigated. Fig. 8 shows a PSD-energy histogram for one of the CLLBC detectors with accompanying FoM values.

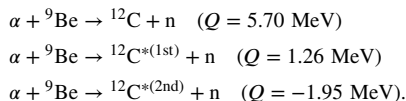
The PSD-energy histogram shows a band over the whole energy range corresponding to  $\gamma$ -rays, that widens in PSD range at low energies. A few islands above the  $\gamma$ -ray band are from  $\alpha$ -particles from  ${}^{227}\text{Ac}$  and daughters, a known contaminant of La-containing scintillators [23, 41]. An island from neutron detection via  ${}^6\text{Li}(n,t)$  is observed at about 3.2 MeVee. Note the unit of MeVee (MeV electron equivalent), as the calibration was done with  $\gamma$ -rays but neutrons are measured.

Obtained results indicate FoM $_{\gamma n}$  values of  $2.73 \pm 0.02$ ,  $2.44 \pm 0.02$ , and  $2.19 \pm 0.02$  for CLLBC detectors 1–3. Interestingly, the best  $\gamma$ -neutron separation is obtained with a detector that exhibited energy peak asymmetry. The FoM $_{\gamma n}$  values are on par with those previously found in literature, ranging from 1.7 [1] to 3.2 [22]. Furthermore, FoM $_{n\alpha}$  values of  $0.75 \pm 0.02$ ,  $0.67 \pm 0.05$ , and  $0.61 \pm 0.06$  were obtained for CLLBC 1–3.

A peak at 1436 keV from the naturally abundant but radioactive lanthanum isotope  ${}^{138}\text{La}$  is also observed, as La is present in CLLBC.

### 3.4.2. Fast-neutron detection via the ${}^6\text{Li}(n,t)$ reaction

An  ${}^{241}\text{Am}^9\text{Be}$  source was used to supply neutrons. The main reactions responsible for neutron production are



Here,  ${}^{12}\text{C}^{*(1st)}$  de-excites through emission of a 4.44 MeV  $\gamma$ -ray, with a half-life of about 42 fs. The five LaBr $_3$  detectors shown in Fig. 2 were used to trigger on the 4.44 MeV  $\gamma$ -ray, while the CLLBC detectors were used to detect the neutron. A measurement was conducted for nearly 13 days on an AmBe source with strength  $7.6 \times 10^4$  n/s.

For each coincident detection, 8 values were recorded: channels A and B, energy A and B, PSD A and B, and timestamps A and B. Interesting data could be filtered by applying suitable cuts to this data. The time difference between coincident detections was recorded and

used to determine the neutron ToF. In turn, the ToF was used to calculate the neutron kinetic energy according to

$$E_n = m_n c^2 \left( \frac{1}{\sqrt{1 - \left( \frac{L}{c \cdot \text{ToF}} \right)^2}} - 1 \right), \quad (2)$$

where  $m_n$  is the neutron mass and  $L$  is the neutron flight distance. This AmBe tagged-neutron ToF technique supplies neutrons between 2–6 MeV and has been used before [42,43]. Fig. 9 shows the PSD-energy histograms of a CLLBC detector when triggering on the 4.44 MeV  $\gamma$ -ray with all five LaBr $_3$  detectors and when neutrons with certain ToF equivalent energies  $E_n$  are selected. Note that to accommodate a higher count rate, PSD was performed with the digitizer onboard FPGA, essentially resulting in a flipped PSD axis with respect to what was presented previously.

In Fig. 9, the  ${}^6\text{Li}(n,t)$  island is present at a PSD parameter value of about 0.14. Although not clearly visible as separate islands, the reactions  ${}^{35}\text{Cl}(n,p)$  and  ${}^{35}\text{Cl}(n,\alpha)$  produce signatures in the same region and occur above a few MeV (see cross sections in Fig. 1). The contribution of these reactions is not well understood in this energy range and needs further study.

Cuts were performed in energy, time, and PSD parameter to select events corresponding to detections via  ${}^6\text{Li}(n,t)$ , with small unavoidable contributions from  ${}^{35}\text{Cl}(n,p)$  and  ${}^{35}\text{Cl}(n,\alpha)$ . The intrinsic neutron detection efficiency was calculated with the help of the partial AmBe neutron spectrum in [44] corresponding to the 4.44 MeV  $\gamma$ -ray coincident emission.

The results in Fig. 10 indicate an intrinsic neutron detection efficiency of about 0.002 (0.2%) in the region 2–6 MeV for all three

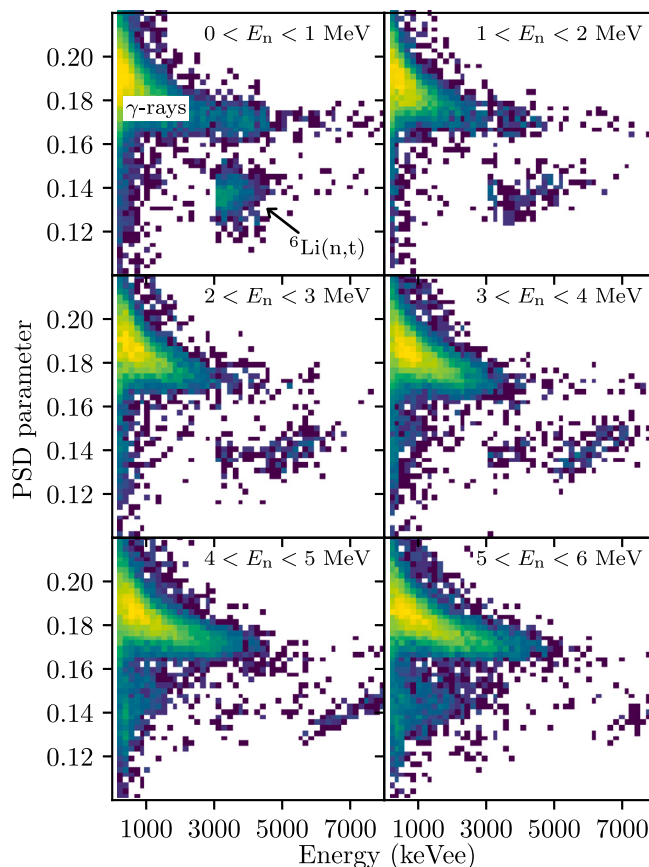


**Fig. 9.** PSD parameter vs. energy response of a CLLBC detector to neutrons in different energy ranges, based on an AmBe measurement. Results are for detector CLLBC (3). Waveform analysis was done with the FPGA.

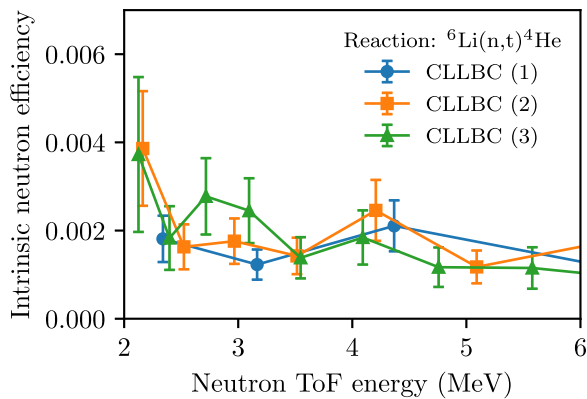


Fig. 10. Intrinsic neutron detection efficiency for the CLLBC detectors using the reaction  ${}^6\text{Li}(n,t)$ .

detectors using the reaction  ${}^6\text{Li}(n,t)$ . A higher efficiency is obtained at around 2 MeV, which is attributed to scattered neutrons. Scattered neutrons have longer flight distances than expected, decreasing the ToF equivalent energy (see Eq. (2)).

### 3.4.3. Fast-neutron detection via $(n,n')$ reactions

A fast neutron can interact with a nucleus in the detector material through an inelastic scattering  $(n,n')$ , exciting the nucleus. When the nucleus de-excites, it may emit a  $\gamma$ -ray of a characteristic energy that can be detected by the detector itself. For CLLBC detectors, peaks from these reactions are visible in the coincident data, as illustrated by Fig. 11. A threshold was imposed to remove 60 keV  $\gamma$ -rays from the AmBe source, but differences in the exact threshold value resulted in some peaks being cut off at low  $E_\gamma$  for CLLBC 3.

The primary origins of the  $\gamma$ -rays are marked in Fig. 11 and correspond to excited states from  $(n,n')$  reactions on Br and La in the detector. There is also a small unmarked contribution to the 276.0 keV peak from  ${}^{79}\text{Br}^*(3\text{rd})$  at 261.3 keV. Cuts on the data were performed for each of the three peaks. The corresponding intrinsic neutron detection efficiencies are presented in Fig. 12.

The intrinsic neutron detection efficiencies of the  $(n,n')$  reactions are about 0.01 (1%), which is larger than for  ${}^6\text{Li}(n,t)$ . This agrees with the cross sections in Fig. 1 between 2–6 MeV. Again, the efficiency is increased at lower energies due to neutron scattering. Furthermore,

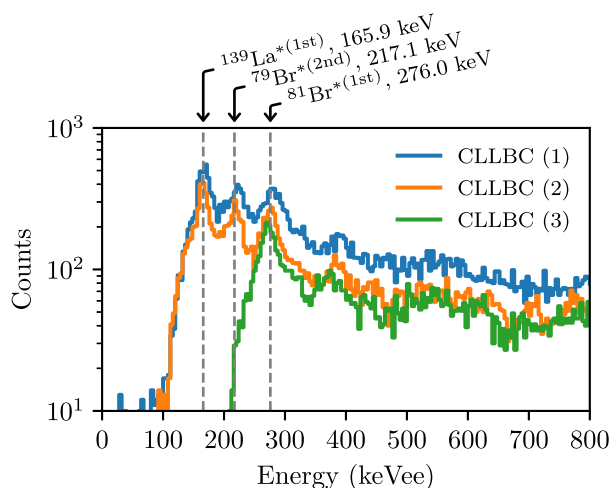


Fig. 11. Energy ( $\gamma$ -equivalent) deposited in the CLLBC detector from the tagged-neutron ToF measurement. Peaks corresponding to states produced from  $(n,n')$  reactions are labeled.

${}^{139}\text{La}^*(1\text{st})$  has a non-negligible half-life of about 1.5 ns, making the ToF appear larger and thus  $E_n$  smaller (see Eq. (2)). This displaces the spectrum to lower neutron energies, making the low-energy efficiency appear larger than it should be.

## 4. Conclusions and outlook

This work has characterized the  $\gamma$ -ray and neutron response of three CLLBC detectors. Results show  $\gamma$ -ray energy resolutions of 3.7%, 4.8%, and 5.7%. The lowest measured resolution is comparable to previously reported performance for CLLBC [1,21,22], while the other cases are affected by scintillator quality issues. The measured intrinsic  $\gamma$ -ray detection efficiencies agree well with Geant4 simulations. Intrinsic FWHM timing resolutions of 1.2 ns, 1.6 ns, and 1.7 ns are obtained, using  ${}^{60}\text{Co}$  and applying a low-energy threshold of  $E_\gamma = 1$  MeV. Intrinsic neutron detection efficiencies in the region 2–6 MeV are approximately 0.2% for the reaction  ${}^6\text{Li}(n,t)$  and 1% for three types of  $(n,n')$  reactions.

Two of the three CLLBC detectors exhibited an energy peak asymmetry, resulting in worse performance, indicating scintillator quality issues and motivating further investigation. The scintillator region causing the asymmetry could be probed by using a collimated  $\gamma$ -ray source and scanning across the scintillator volume. It is also suggested to investigate whether the asymmetry is reflected by the shape of the waveform, which could be used to reduce the asymmetry by selecting a different pulse integration region.

In this work, the neutron detection reaction  ${}^6\text{Li}(n,t)$  and three types of  $(n,n')$  followed by  $\gamma$ -ray emission were employed. Although previous work identified the reaction  ${}^{35}\text{Cl}(n,p)$  in CLLBC [1], this signature was not observed clearly in this work due to the use of non-monoenergetic neutrons. Using tagged AmBe neutrons of  $E_n = 2$ –6 MeV, this signature is spread out over an energy range, making identification difficult and possibly resulting in overlaps with other signatures. Measurements with quasi-monoenergetic neutrons produced at the JRC-Geel MONNET [45] accelerator facility are planned, which would facilitate searching for this signature. Another reaction of interest is  ${}^{35}\text{Cl}(n,\alpha)$ , which has a comparable cross section and has been observed in the elpasolite scintillator CLYC before [4,46].

To measure the intrinsic neutron detection efficiency over a wider neutron energy range, measurements with a  ${}^{252}\text{Cf}(sf)$  neutron source are suggested. By utilizing the whole PFNS and triggering on a fission fragment in an ionization chamber, the ToF equivalent energy could be utilized in a similar way to the AmBe source. In particular, with neutrons below 1 MeV, the  ${}^6\text{Li}(n,t)$  cross section is large, allowing for better statistics.

Alternatively, by tagging on 60 keV  $\gamma$ -rays from  ${}^{241}\text{Am}$ , the whole AmBe spectrum becomes available. However, in such cases one needs to consider the self-absorption of  $\gamma$ -rays in the source when determining the efficiency, something that can be neglected for the 4.44 MeV  $\gamma$ -ray.

In conclusion, CLLBC is suitable for applications, where both  $\gamma$ -ray and neutron detection capabilities are needed. Through PSD and ToF techniques,  $\gamma$ -ray and neutron detections can be discriminated.

## Declaration of competing interest

The authors declare that they have no known competing financial interests or personal relationships that could have appeared to influence the work reported in this paper.

## Acknowledgments

This work has been partially supported by the ENEN2plus project (HORIZON-EURATOM-2021-NRT-01-13 101061677) funded by the European Union.

This work was supported by the Swedish Research Council (VR ref. no. 2019-05385).

One of the authors (A. O.) would like to acknowledge the support by the Romanian Ministry of Research and Innovation under research contract PN 23 21 01 06.

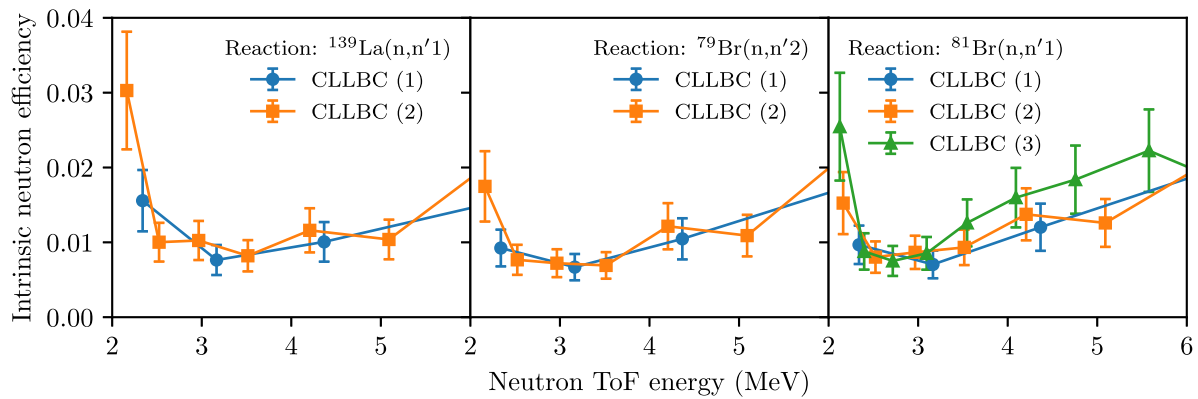


Fig. 12. Intrinsic neutron detection efficiencies for the CLLBC detectors using three types of  $(n,n')$  reactions followed by  $\gamma$ -ray emission.

## Data availability

Data will be made available on request.

## References

- [1] U. Shirwadkar, R. Hawrami, J. Glodo, E.V.D. Van Loef, K.S. Shah, IEEE NSS-MIC 2012 (2012) 1963.
- [2] J. Glodo, R. Hawrami, E.V.D. Van Loef, U. Shirwadkar, K.S. Shah, IEEE Trans. Nucl. Sci. 59 (2012) 2328.
- [3] N. D'Olympia, P. Chowdhury, C.J. Lister, J. Glodo, R. Hawrami, K. Shah, U. Shirwadkar, Nucl. Instr. Methods A 714 (2013) 121.
- [4] A. Giaz, N. Blasi, C. Boiano, S. Brambilla, F. Camera, C. Cattadori, S. Ceruti, F. Gramegna, T. Marchi, I. Mattei, A. Mentana, B. Million, L. Pellegri, M. Rebai, S. Riboldi, F. Salamida, M. Tardocchi, Nucl. Instr. Methods A 825 (2016) 51.
- [5] A. Oberstedt, R. Billnert, S. Oberstedt, Nucl. Inst. Methods A 708 (2013) 7.
- [6] A. Ebran, O. Roig, V. Méot, O. Delaune, Nucl. Inst. Methods A 768 (2014) 124.
- [7] N.V. Kornilov, I. Fabry, S. Oberstedt, F.-J. Hamsch, Nucl. Inst. Methods A 599 (2014) 226.
- [8] Nuclear Data High Priority Request List of the NEA (Req. ID: H.3, H.4), <https://www.oecd-nea.org/dbdata/hprl/hprlview.pl?ID=421> and <https://www.oecd-nea.org/dbdata/hprl/hprlview.pl?ID=422>.
- [9] R. Billnert, F.-J. Hamsch, A. Oberstedt, S. Oberstedt, Phys. Rev. C 87 (2013) 024601.
- [10] A. Oberstedt, T. Belgya, R. Billnert, R. Borcea, T. Bryś, W. Geerts, A. Göök, F.-J. Hamsch, Z. Kis, T. Martinez, S. Oberstedt, L. Szentmiklósi, K. Takács, M. Vidali, Phys. Rev. C 87 (2013) 051602(R).
- [11] S. Oberstedt, R. Billnert, T. Belgya, T. Bryś, I.W. Geerts, C. Guerrero, F.-J. Hamsch, Z. Kis, A. Moens, A. Oberstedt, G. Sibbens, L. Szentmiklósi, D. Vanleeuw, M. Vidali, Phys. Rev. C 90 (2014) 024618.
- [12] A. Oberstedt, R. Billnert, F.-J. Hamsch, S. Oberstedt, Phys. Rev. C 92 (2015) 014618.
- [13] S. Oberstedt, A. Oberstedt, A. Gatera, A. Göök, F.-J. Hamsch, A. Moens, G. Sibbens, D. Vanleeuw, M. Vidali, Phys. Rev. C 93 (2016) 054603.
- [14] A. Gatera, T. Belgya, W. Geerts, A. Göök, F.-J. Hamsch, M. Lebois, B. Maróti, A. Moens, A. Oberstedt, S. Oberstedt, F. Postelt, L. Qi, L. Szentmiklósi, G. Sibbens, D. Vanleeuw, M. Vidali, F. Zeiser, Phys. Rev. C 95 (2017) 064609.
- [15] L. Qi, M. Lebois, J.N. Wilson, A. Chatillon, S. Courtin, G. Fruet, G. Georgiev, D.G. Jenkins, B. Laurent, L. Le Meur, A. Maj, P. Marini, I. Matea, L. Morris, V. Nanal, P. Napiorkowski, A. Oberstedt, S. Oberstedt, C. Schmitt, O. Serot, M. Stanoiu, B. Wasilewska, Phys. Rev. C 98 (2018) 014612.
- [16] L. Qi, C. Schmitt, M. Lebois, A. Oberstedt, S. Oberstedt, J.N. Wilson, A. Al-Adili, A. Chatillon, D. Choudhury, A. Gatera, G. Georgiev, A. Göök, B. Laurent, A. Maj, I. Matea, S.J. Rose, B. Wasilewska, F. Zeiser, Eur. Phys. J. A 56 (2020) 98.
- [17] A. Oberstedt, A. Gatera, A. Göök, S. Oberstedt, Eur. Phys. J. A 56 (2020) 196.
- [18] A. Oberstedt, M. Lebois, S. Oberstedt, L. Qi, J.N. Wilson, Eur. Phys. J. A 56 (2020) 236.
- [19] M. Travar, V. Piau, A. Göök, O. Litaize, J. Nikolov, A. Oberstedt, S. Oberstedt, J. Enders, M. Peck, W. Geerts, M. Vidali, Phys. Lett. B 817 (2021) 136293.
- [20] D.A. Brown, et al., Nucl. Data Sheets 148 (2018) 1.
- [21] P.P. Guss, T.G. Stampahar, S. Mukhopadhyay, A. Barzilov, A. Guckes, Proc. SPIE Radiat. Detect. 9215 (2014).
- [22] R. Hawrami, L.S. Pandian, E. Ariesanti, J. Glodo, J. Finkelstein, J. Tower, K. Shah, IEEE Trans. Nucl. Sci. 63 (2016) 509.
- [23] G. Hull, F. Camera, G. Colombi, M. Josselin, B. Million, N. Blasi, Nucl. Inst. Methods A 925 (2019) 70.
- [24] K.E. Mesick, K.D. Bartlett, D.D.S. Coupland, L.C. Stonehill, Nucl. Inst. Methods A 948 (2019) 162774.
- [25] N. Kaneshige, L.S. Pandian, K. Werra, J. Tower, J. Glodo, E. Johnson, M.P. Dion, I. Garishvili, G. Westphal, L.G. Worrall, M.R. Squillante, K. Shah, IEEE Trans. Nucl. Sci. 70 (2023) 1357.
- [26] J.M.C. Brown, L. Chartier, D. Boardman, J. Barnes, A. Flynn, Nucl. Inst. Methods A 1057 (2023) 168726.
- [27] F. Liang, J. Smith, IEEE Trans. Nucl. Sci. 67 (2023) 927.
- [28] V. Piau, Predictive Calculations of Fission Observables from Dedicated Experiments (Ph.D. thesis), Université Grenoble Alpes, 2022.
- [29] CLLBC neutron / Gamma scintillation crystals, 2024, <https://scionix.nl/>.
- [30] DT5730 / DT5730s 8 channel 14 bit 500 MS/s digitizer, 2024, <https://www.caen.it/products/dt5730/>.
- [31] ABCD: Acquisition and Broadcast of Collected Data, <https://github.com/ec-jrc/abcd>.
- [32] C.L. Fontana, N. Tuccori, F.E. Pino, M. Lunardon, L. Stevanato, S. Moretto, J. Instrum. 15 (2020) P06020.
- [33] Z. Janout, S. Pospíšil, M. Vobecký, J. Radioanal. Chem. 56 (1980) 71.
- [34] InterSpec, <https://github.com/sandialabs/InterSpec>.
- [35] G.R. Gilmore, Practical Gamma-Ray Spectrometry, second ed., John Wiley & Sons, Ltd, 2008.
- [36] S. Agostinelli, et al., Nucl. Inst. Methods A 506 (2003) 250.
- [37] J. Allison, et al., IEEE Trans. Nucl. Sci. 53 (2006) 270.
- [38] J. Allison others, Nucl. Inst. Methods A 835 (2016) 186.
- [39] S. Pommé, Appl. Radiat. Isot. 66 (2008) 941.
- [40] T. Liu, J. Chen, P. Zhu, Y. Li, G. Zhang, Appl. Radiat. Isot. 65 (2007) 1318.
- [41] J.K. Hartwell, R.J. Gehrke, Appl. Radiat. Isot. 63 (2005) 223.
- [42] J. Scherzinger, J.R.M. Annand, G. Davatz, K.G. Fissum, U. Gendotti, R. Hall-Wilton, E. Håkansson, R. Jebali, K. Kanaki, M. Lundin, B. Nilsson, A. Rosborge, H. Svensson, Appl. Radiat. Isot. 98 (2015) 74.
- [43] H. Ito, K. Wada, T. Yano, Y. Hino, Y. Ommura, M. Harada, A. Minamino, M. Ishitsuka, Nucl. Inst. Methods A 1057 (2023) 168701.
- [44] F. De Guarrini, R. Malaroda, Nucl. Inst. Methods 92 (1971) 277.
- [45] C.L. Fontana, C. Bonaldi, W. Geerts, M. Macias, M. Vidali, S. Oberstedt, EPJ Web Conf. 284 (2023) 06002.
- [46] N. D'Olympia, P. Chowdhury, E.G. Jackson, C.J. Lister, Nucl. Inst. Methods A 763 (2014) 433.